(Preprint) AAS 17-204

VALIDATION OF A LOW-THRUST MISSION DESIGN TOOL USING OPERATIONAL NAVIGATION SOFTWARE

Jacob A. Englander*
Jeremy M. Knittel†
Ken Williams‡
Dale Stanbridge§
Donald H. Ellison¶

Design of flight trajectories for missions employing solar-electric propulsion requires a suitably high-fidelity design tool. In this work, the Evolutionary Mission Trajectory Generator (EMTG) is presented as a medium-high fidelity design tool that is suitable for mission proposals. EMTG is validated against the high-heritage deep-space navigation tool MIRAGE, demonstrating both the accuracy of EMTG's model and an operational mission design and navigation procedure using both tools. The validation is performed using a benchmark mission to the Jupiter Trojans.

INTRODUCTION

The design of trajectories for interplanetary missions requires a highly specialized toolset. This is especially true for missions employing solar-electric propulsion (SEP). Several medium-fidelity tools exist that are suitable for early mission formulation, including EMTG [1, 2], Mission Analysis Low-Thrust Optimization (MALTO) [3], Gravity Assisted Low-thrust Local Optimization Program (GALLOP) [4], and Parallel Global Multiobjective Optimizer (PaGMO) [5]. These tools allow a designer to rapidly determine the key parameters of a mission concept, including flight time, propellant mass, delivered dry mass, *etc.*, but the trajectories generated by these tools only roughly resemble those that a spacecraft might actually fly. There are also several flight-fidelity low-thrust tools, including Copernicus [6] and Mystic [7].

In the mission proposal stage, medium-fidelity is often sufficiently accurate to be used for high-level mission and systems trades. However, when it comes time to submit a proposal, it is a good idea to provide at least one trajectory that is designed to a higher level of fidelity. The flight-fidelity tools that produce these solutions, however, require a great deal of human analyst time that may not be available or affordable in the context of a proposal. In addition, the flight-fidelity tools are not always readily available to all teams wishing to submit a proposal. An intermediate level of design fidelity that is easy and inexpensive to use and also readily available to all potential users is therefore highly desirable. Such a "medium-high" fidelity tool should integrate the equations of motion rather than approximating them and its force model should include reasonably high fidelity models of propulsion and power systems as well as significant orbit perturbations such as third-body gravity and solar radiation pressure (SRP). Such a tool is sufficient to ensure that a proposed trajectory is actually feasible and is not an artifact of the low-fidelity and medium-fidelity models available in most preliminary design tools. However, before such a medium-high fidelity tool can be trusted, it must be validated against a high-heritage navigation tool that might be used to actually fly the mission.

*Aerospace Engineer, Navigation and Mission Design Branch, NASA Goddard Space Flight Center, Member AAS
†Aerospace Engineer, Navigation and Mission Design Branch, NASA Goddard Space Flight Center
‡Flight Director, Space Navigation and Flight Dynamics Practice, KinetX Aerospace, Simi Valley, California, 93065
§Senior Navigation Analyst, Space Navigation and Flight Dynamics Practice, KinetX Aerospace, Simi Valley, California, 93065
¶Ph.D. Candidate, Department of Aerospace Engineering, University of Illinois at Urbana-Champaign

In this work, the EMTG [1, 2] is presented as a tool for medium-high fidelity trajectory design, that is suitable for mission proposals. The finite-burn low-thrust (FBLT) [8] force model is extended to include third-body perturbations and solar radiation pressure. The resulting medium-high fidelity design tool is then validated against the operational navigation tool Multiple Interferometric Ranging Analysis using GPS Ensemble (MIRAGE). MIRAGE is a licensed version of the Double-Precision Trajectory and Orbit Determination Program (DPTRAJ/ODP) originally developed at JPL to support high-fidelity orbit determination, trajectory propagation and maneuver planning [9]. MIRAGE has flight heritage from the 1970s to the present day and has been used to navigate many deep-space missions, including NEAR, Stardust, Genesis, and many other missions at JPL, and, more recently at KinetX, MESSENGER, New Horizons, and OSIRIS-REx. Most relevant to this work, MIRAGE was used to navigate the Deep Space 1 mission, which employed solar electric propulsion. MIRAGE is therefore an ideal environment in which to check the accuracy of EMTG's FBLT mode.

THE FINITE-BURN LOW-THRUST TRAJECTORY MODEL

The FBLT transcription divides a continuous-thrust spacecraft trajectory into N_{p} phases, each consisting of N control decision segments. The spacecraft's state ($\mathbf{X}$) is propagated from either phase boundary to the center of the phase. A constraint is applied at the "match point" that ensures state continuity to some numerical tolerance.

$$\mathbf{c}^{\dagger} = \mathbf{X}_B^{\dagger} - \mathbf{X}_F^{\dagger} = \begin{bmatrix} \mathbf{r}_B^{\dagger} - \mathbf{r}_F^{\dagger} \\ \dot{\mathbf{r}}_B^{\dagger} - \dot{\mathbf{r}}_F^{\dagger} \\ m_B^{\dagger} - m_F^{\dagger} \end{bmatrix} = \mathbf{0} \tag{1}$$

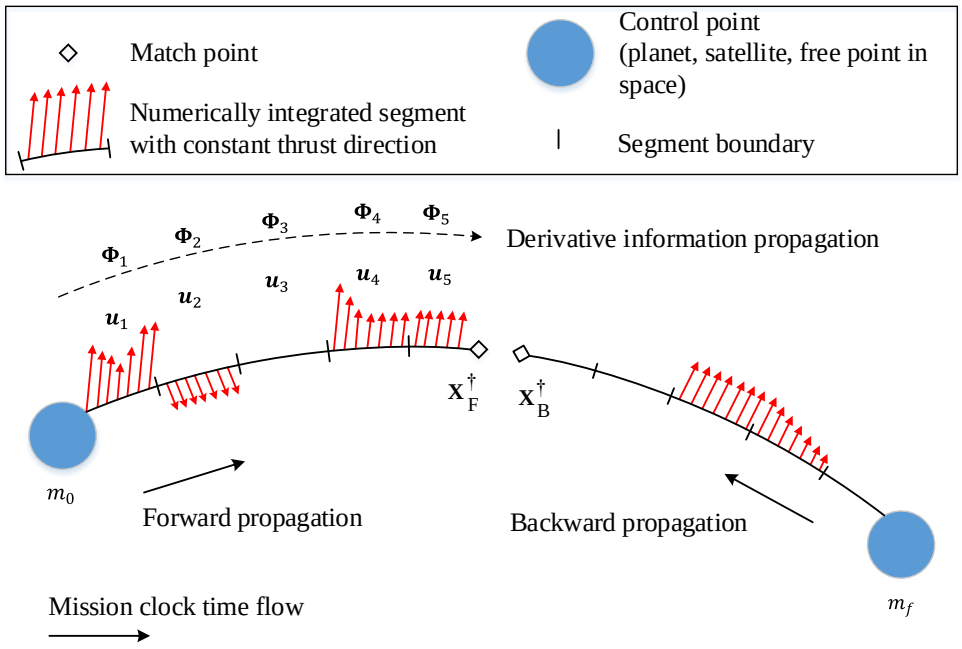

Figure 1: An FBLT phase with $N = 10$ control segments.

Partial derivatives of this constraint are computed using augmented state transition matrices (STM) (Eq. (2)) that are computed using the FBLT physics engine. These STMs are also useful for performing navigation

tasks such as filtering and orbit determination (OD).

$$\mathbf{\Phi}(t,t_0) = \begin{bmatrix} \frac{\partial \mathbf{r}}{\partial \mathbf{r}_0} & \frac{\partial \mathbf{r}}{\partial \dot{\mathbf{r}}_0} & \frac{\partial \mathbf{r}}{\partial m_0} & \frac{\partial \mathbf{r}}{\partial \mathbf{u}_0} \\ \frac{\partial \dot{\mathbf{r}}}{\partial \mathbf{r}_0} & \frac{\partial \dot{\mathbf{r}}}{\partial \dot{\mathbf{r}}_0} & \frac{\partial \dot{\mathbf{r}}}{\partial m_0} & \frac{\partial \dot{\mathbf{r}}}{\partial \mathbf{u}_0} \\ \hline \frac{\partial m}{\partial \mathbf{r}_0} & \frac{\partial m}{\partial \dot{\mathbf{r}}_0} & \frac{\partial m}{\partial m_0} & \frac{\partial m}{\partial \mathbf{u}_0} \\ \mathbf{0}_{3\times 3} & \mathbf{0}_{3\times 3} & \mathbf{0}_{3\times 1} & \mathbb{I}_{3\times 3} \end{bmatrix} \tag{2}$$

The FBLT transcription models the effects of perturbing forces from sources other than the central body's gravity and the spacecraft's thruster, such as other gravitating bodies and solar radiation pressure SRP, by directly incorporating them into the equations of motion. This is known as Cowell's method of special perturbations. The differential equations of motion governing a continuously thrusting spacecraft in orbit around a central body subject to gravitational forces from massive bodies and solar radiation pressure, using a spherical cannonball model [10], are:

$$\ddot{\mathbf{r}} = -\frac{G\left(\cancel{m}^{0} + m_{\text{cb}}\right)}{r^2}\frac{\mathbf{r}}{r} - \sum_{\text{i}} G\, m_{\text{i}} \left(\frac{\mathbf{r} - \mathbf{r}_{\text{i}}}{\|\mathbf{r} - \mathbf{r}_{\text{i}}\|^3} + \frac{\mathbf{r}_{\text{i}}}{r_{\text{i}}^3} \right) + \frac{C_r A_s K \phi}{c\, r_{s/\odot}^2} \frac{\mathbf{r}_{s/\odot}}{r_{s/\odot}} + \frac{D\, T}{m}\mathbf{u} \tag{3}$$

$$\dot{m} = -\|\mathbf{u}\|\, D\, \dot{m}_{\text{max}} \tag{4}$$

where G is the universal gravitational constant, m is the mass of the spacecraft, m_{cb} is the mass of the central gravitational body to which the inertial reference frame is fixed, m_{i} is the mass of the i^{th} gravitational body, $\mathbf{r}$ is the position vector of the spacecraft with respect to the central body and $\mathbf{r}_{\text{i}}$ is the position vector of the i^{th} body with respect to the central body. The vectors $\mathbf{r}_{\text{i}}$ and $\mathbf{r}_{\odot}$ are obtained from ephemeris calls. The vector $\mathbf{r}_{\text{s}/\odot}$ is the position vector of the spacecraft with respect to the sun and $\mathbf{r}_{\text{s/i}}$ is the position vector of the spacecraft with respect to the i^{th} gravitational body, both expressed in the coordinates of the inertial frame attached to the central body, i.e.

$$\mathbf{r}_{\text{s}/\odot} = \mathbf{r} - \mathbf{r}_{\odot} \tag{5}$$

Regarding the variables associated with radiation pressure, C_r is the coefficient of reflectivity on the interval $[0, 2]$, A_s is the spacecraft area exposed to sunlight, K is the total percentage of the sun seen by the spacecraft ($[0, 1]$), ϕ is the solar flux and c is the speed of light in a vacuum. The thruster variable $\mathbf{u}$ is a throttle scaling vector whose three components are selected by the optimizer on the range $[-1, 1]$, D is the thruster duty cycle (modeled continuously), T is the instantaneous thrust of the electric motor and $\dot{m}_{\text{max}}$ is the maximum instantaneous mass flow rate of the propellant through the motor. Note that in Equation (3) the mass of the spacecraft is neglected in the first term since $m_{\text{cb}} >> m$.

The vector geometry of this problem is illustrated in Figure 2. The diagram on the left depicts the general case, where the central body need not be the sun, whereas the right hand diagram shows how the configuration simplifies for a heliocentric trajectory.

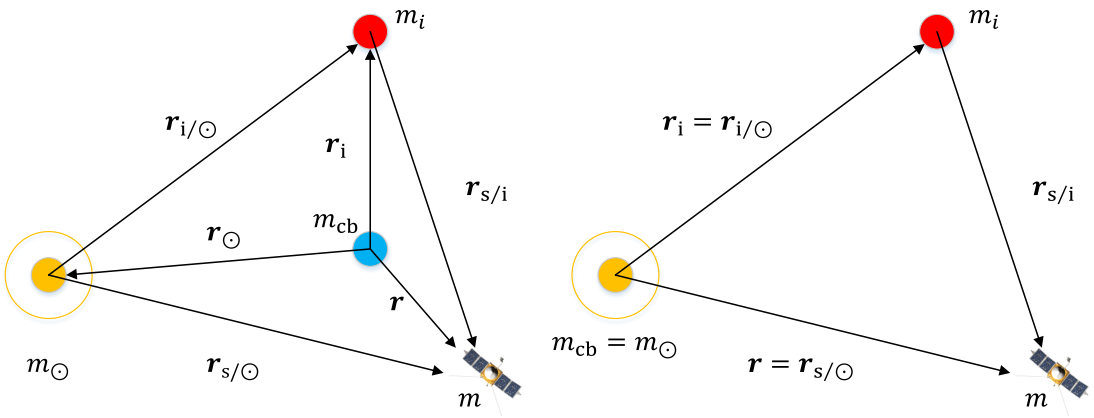

Figure 2: Vector diagrams for the general central body case and the simplified heliocentric case.

For the situation shown on the left in Figure 2 the sun is included for two reasons, despite the fact that it is not the central body. The first reason is that for most mission designs, the sun would almost certainly be included in the problem dynamics (the summation in Equation (3)) due to its gravitational dominance in the solar system. The second reason is that for accurate solar-electric propulsion modeling, the position of the spacecraft with respect to the sun must be tracked at all times throughout the optimization since many of the quantities in Eq. (3) and (4) are dependent on the solar flux at any instant in time, i.e.

$$T = T(r_{s/\odot}(\mathbf{r})) \quad \dot{m}_{\max} = \dot{m}_{\max}(r_{s/\odot}(\mathbf{r})) \tag{6}$$

SPACECRAFT POWER SYSTEM MODELING

For a spacecraft using a solar electric propulsion (SEP) system, the maximum amount of thrust that the system can produce depends on the power available, which depends on its distance from the sun. This must be modeled in the low-thrust global optimization even at the preliminary design stage. Typically trajectory design engineers are supplied with polynomial representations of the thrust and mass flow rate of a given thruster, *e.g.*,

$$T = e_T P_{\text{eff}}^4 + d_T P_{\text{eff}}^3 + c_T P_{\text{eff}}^2 + b_T P_{\text{eff}} + a_T \tag{7}$$

$$\dot{m}_{\max} = e_m P_{\text{eff}}^4 + d_m P_{\text{eff}}^3 + c_m P_{\text{eff}}^2 + b_m P_{\text{eff}} + a_m \tag{8}$$

where P_{eff} is the power available to each thruster,

$$P_{\text{eff}} = P/N_{\text{active}} \tag{9}$$

and N_{active} is the number of thrusters firing at any point in time. Equations (7) and (8) are valid over a range $[P_{\min}, P_{\max}]$ where $P_{\min}$ represents the minimum amount of power necessary to turn on the thruster's power processing unit (PPU) at the lowest setting and $P_{\max}$ represents the maximum amount of power that the PPU can safely accommodate. The total power available to the electric propulsion system (P) is the difference between the power generated by the spacecraft $P_{\text{generated}}$ and the power required to operate the spacecraft bus $P_{\text{s/c}}$,

$$P = (1 - \delta_{\text{power}})\,(P_{\text{generated}} - P_{\text{s/c}}) \tag{10}$$

where δ_{power} is the propulsion power margin. In this work, the power delivered by a solar array is given by [11]:

$$P_{\text{generated}} = \frac{P_0}{r_{s/\odot}^2}\left(\frac{\gamma_0 + \gamma_1/r_{s/\odot} + \gamma_2/r_{s/\odot}^2}{1 + \gamma_3 r_{s/\odot} + \gamma_4 r_{s/\odot}^2}\right) \tag{11}$$

where the γ_i are solar panel coefficients typically determined from experimental data, $r_{s/\odot}$ is the distance between the sun and the spacecraft in Astronomical Unit (AU) and P_0 is the "base power" delivered by the array at 1 AU. P_0 is in turn a function of the time since launch,

$$P_0 = P_{0\text{-BOL}} (1 - \tau)^t \tag{12}$$

where $P_{0\text{-BOL}}$ is the base power delivered by the array at 1 AU on the day of launch, τ is the decay rate of the solar arrays measured as a percentage per year, and t is the time since launch in years.

The power required by the spacecraft bus $P_{s/c}$ is also modeled as a polynomial,

$$P_{s/c} = a_{s/c} + b_{s/c}/r_{s/\odot} + c_{s/c}/r_{s/\odot}^2 \tag{13}$$

where $a_{s/c}$, $b_{s/c}$, and $c_{s/c}$ are specified by the mission designer.

APPLICATION:NAUPLIUS-ODYSSEUS MISSION

A notional SEP mission to the Trojan asteroids Nauplius and Odysseus is used as the benchmark case to compare EMTG and MIRAGE. This benchmark is particularly timely because the "Trojan Tour and Rendezvous" is listed as one of the acceptable targets in the New Frontiers 4 Announcement of Opportunity that was recently released by NASA [12]. As a mission of current interest, the Trojan Tour and Rendezvous is an ideal case with which to validate a new design tool that may be used to propose such missions. The Announcement of Opportunity states that the Trojan Tour and Rendezvous "is intended to examine two or more small bodies sharing the orbit of Jupiter, including one or more flybys followed by an extended rendezvous with a Trojan object." Accordingly, our benchmark mission performs a flyby of the magnitude 10.7 Trojan 9712 Nauplius before rendezvousing with 1143 Odysseus, which at magnitude 7.93 is one of the largest Trojans. This benchmark is appropriate for validating EMTG against MIRAGE and also provides a test case for an operational validation process that could be used for any mission or mission proposal.

The assumptions for the benchmark mission to Nauplius and Odysseus are listed in Table 1. Table 3 lists the major events in the mission, and Figure 3 is a plot of the optimal trajectory. The specific force model settings used in the comparison are given in Table 4 provided in the next section.

Table 1: Assumptions for the benchmark mission to Nauplius and Odysseus

Option	Value
Launch window	1/1/2024 - 12/31/2024
Flight time upper bound	12 years
Arrival conditions	Nauplius: flyby Odysseus: rendezvous
Launch vehicle	Atlas V 551
Launch asymptote declination bounds	$[-28.5, 28.5]$ (Kennedy Space Center)
Post-launch/Pre-flyby/Post-flyby coast durations	60/30/30 days
Solar array P_0	40 kW
Solar array coefficients γ_i	$[1, 0, 0, 0, 0]$
Spacecraft power coefficients $a_{s/c} - c_{s/c}$	$[0.8, 0, 0]$
Propulsion system	2 NEXT in "high-Thrust" mode [13]
Throttle logic	minimum number of thrusters
Duty cycle	90%
Power margin	15%
Number of segments per phase	40

The NEXT thruster coefficients for use in Eq. (7) and (8) are provided in Table 2. The multi-thruster logic used for this problem is provided in Algorithm1.

Table 2: Thruster performance parameters.

Parameter	NEXT TT11 [13] High-Thrust
$\{a_T, b_T, c_T, d_T, e_T\}$ (mN)	$\{11.9388817, 16.0989424, 11.4181412, -2.04053417, 0.101855017\}$
$\{a_m, b_m, c_m, d_m, e_m\}$ (mg/s)	$\{2.75956482, -1.71102132, 1.21670237, -0.207253445, 0.011021367\}$
$[P_{\text{min}}, P_{\text{max}}]$ (kW)	[0.64, 7.36]

Algorithm 1 Multi-Thruster Logic:
Minimum Number of Thrusters

$N_{\text{active}} = N_{\text{available}}$
if $P \geq P_{\text{min}}$ **then**
  for $n = N_{\text{available}}; n > 0; --n$ **do**
    if $P \leq nP_{\text{max}}$ **then**
      $N_{\text{active}} = n$
      break
    end if
  end for
else
  $N_{\text{active}} = 0$
end if

Table 3: Significant events in the Nauplius-Odysseus mission

Event #	Date	Event	Location	v_∞ (km/s)	Mass (kg)
1	12/31/2024	launch	Earth	5.587	3256.2
2	7/13/2033	intercept	9712 Nauplius	2.229	1852.4
3	12/31/2036	LT rendezvous	1143 Odysseus		1653.1

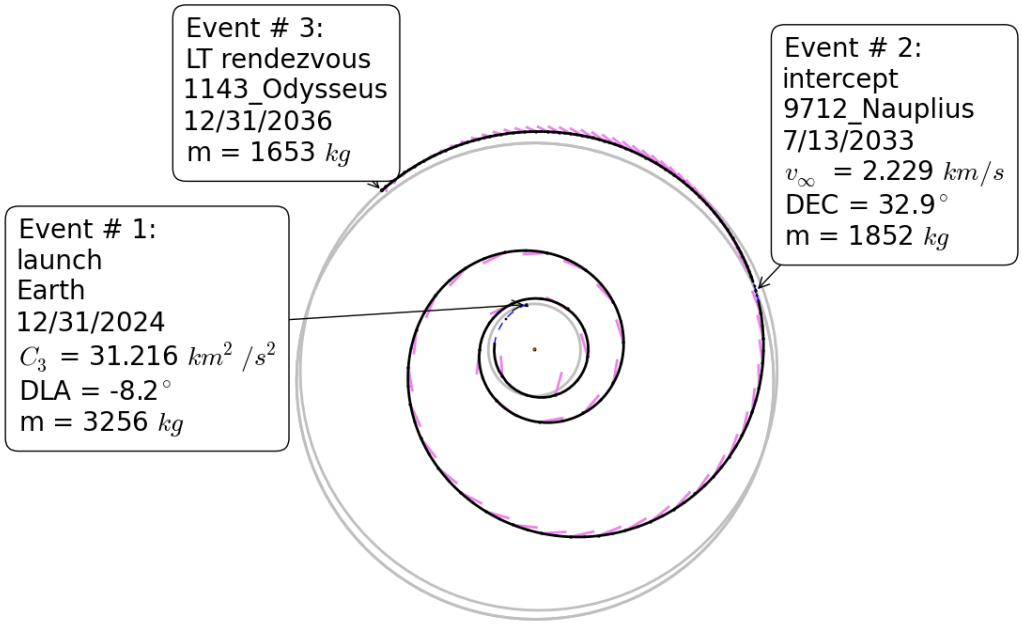

Figure 3: Optimal trajectory to Nauplius and Odysseus, from EMTG

TRAJECTORY VERIFICATION

The low-thrust trajectory generated by EMTG can be converted into a near-equivalent trajectory created by the MIRAGE navigation software. This is done for two reasons: to perform independent verification and validation of the EMTG propagation and to create a database suitable for conducting orbit determination (OD) covariance analysis and trajectory prediction and management during flight operations. MIRAGE models each thrust segment produced by EMTG as a long finite-burn based on a specified thrust profile and direction. The SEPV module of MIRAGE is employed to search for a Δv that achieves the target position state at the end of each thrust arc. To avoid overlap of finite-burn segments, the actual thrust arc, as modeled by MIRAGE, is shortened by up to one hour to allow margin for searching in the Δv. This slight foreshortening amounts to a tiny fraction of the overall thrust arc. Because of small mismatches in force models between the two sets of software, small adjustments or tweaks to the thrust level are required to achieve convergence of spacecraft state, including velocity and mass, as well as position.

For the scenario used as a test case for this study, force models and planetary ephemerides used by EMTG and MIRAGE were simplified as much as possible, as shown in Table 4, to facilitate comparison of results.

Table 4: Simplified force model assumptions used for the EMTG-MIRAGE comparison.

Category	Model	Notable Details
Planetary ephemerides	DE433	• Available bodies (SPICE ID): SUN (10), MERCURY BARYCENTER (1), MERCURY(199), VENUS BARYCENTER (2), VENUS (299), EARTH BARYCENTER (3), EARTH (399), MOON (301), MARS BARYCENTER (4), MARS (499), JUPITER BARYCENTER (5), SATURN BARYCENTER (6), URANUS BARYCENTER (7), NEPTUNE BARYCENTER (8), PLUTO BARYCENTER (9)
		• Time span (ET or TDB): 1899 DEC 04 00:00:00 - 2050 OCT 17 00:00:00
Gravity	Sun, Earth and Jupiter only μ $[km^3/s^2]$	• $\mu_\odot$ = 1.32712440041939E+11
		• $\mu_\oplus$ = 3.98694790080000E+05
		• $\mu_{\mathbb{4}}$ = 1.26686510964000E+08
Solar radiation pressure	Spacecraft bus	• A_s = 114.1 m^2
		• C_r = 1.0
		• ϕ = 1.015242216E+08 $\frac{kg\ km^3}{m^2 s^2}$ equivalent to solar luminosity $L_\odot = 1360 \frac{W}{m^2}$

Accelerations associated with specific forces were checked and model inputs tuned to ensure good agreement between the two software sets. It is understood that for an actual flight mission, complexity and fidelity of models would be increased systematically to preserve the consistency of models between the two software sets.

Figures 4-6 provide deviations of the MIRAGE derived states relative to EMTG for the Earth-Nauplius phase of the representative low-thrust mission. The red dashed lines indicate a point within a specific thrust arc where power limitations necessitated powering down one of the active thrusters. These changes were modeled in terms of thrust and mass flow changes, which can be characterized in MIRAGE as quartic and cubic polynomials of elapsed time, respectively. Since these inflection points were so approximated, this engendered certain state discrepancies, as shown in Figures 4-6. Nevertheless, the resultant maximum differ-

ence in targeted position over the entire trajectory phase was only 87.3 m. The maximum velocity difference of 1.17 m/s coincided with one of the thrust mode changes, but this discrepancy dissipated exponentially over the remainder of the trajectory phase, resulting in a final mass difference of 742 g, a final velocity difference of about 15 cm/s and an overall discrepancy in Δv usage of only 2.24 m/s out of a total of 17.34 km/s of total Δv expended, well within the operational tolerances that could be anticipated for such a mission.

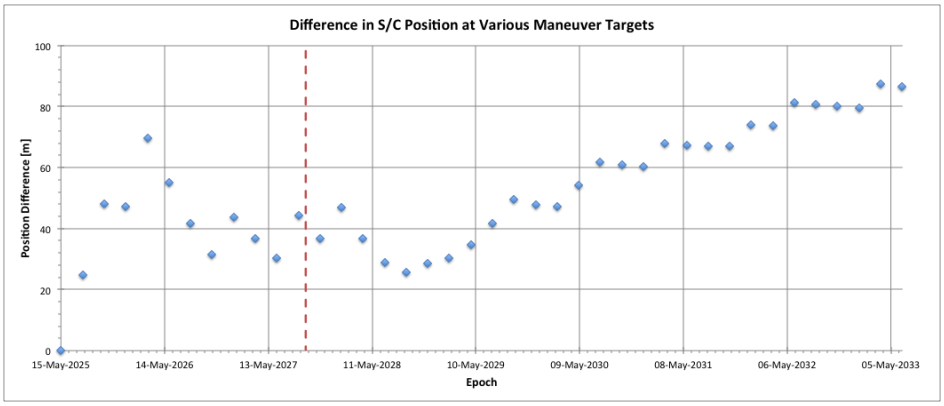

Figure 4: Differences in propagated spacecraft position of MIRAGE relative to EMTG for the Earth-Nauplius phase.

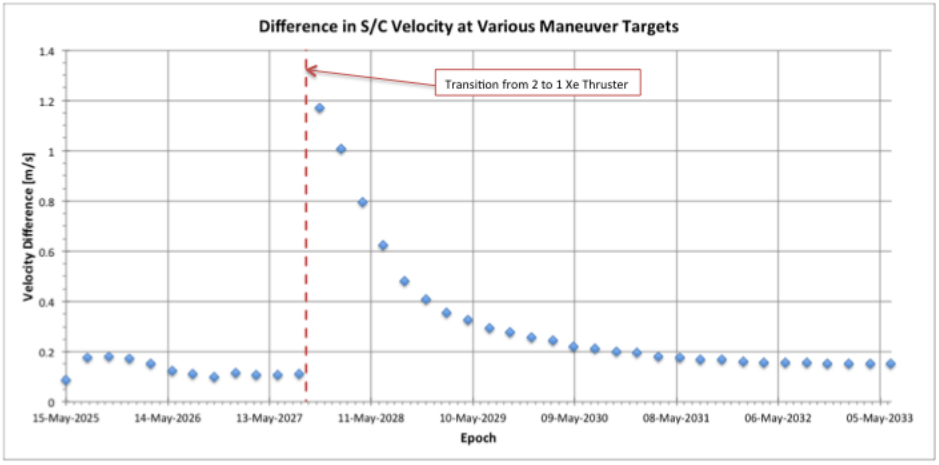

Figure 5: Differences in propagated spacecraft velocity of MIRAGE relative to EMTG for the Earth-Nauplius phase.

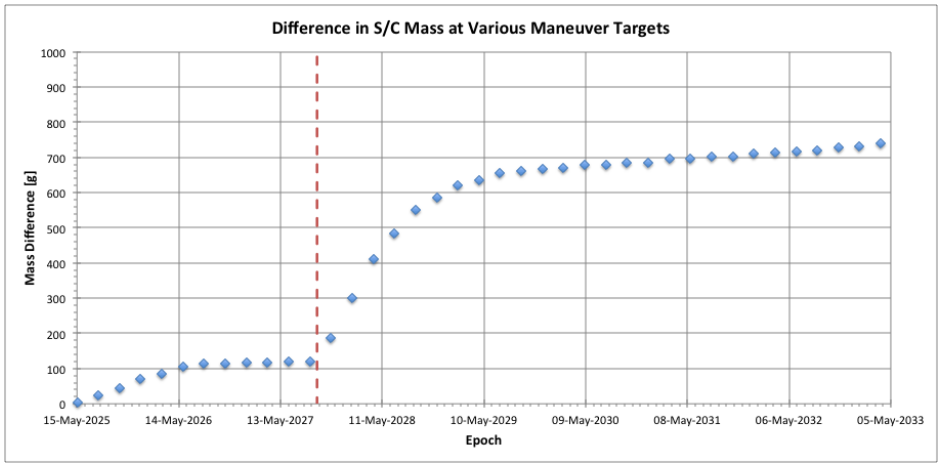

Figure 6: Differences in propagated spacecraft mass of MIRAGE relative to EMTG for the Earth-Nauplius phase.

Also, if the problematic thrust arc is partitioned at the point where one of the thrusters is deactivated, the agreement between EMTG and MIRAGE is somewhat improved. Although the maximum position discrepancy is now 162.3 m, the maximum velocity difference is now reduced to 69.6 cm/s, the final mass difference falls to 449 g, and the overall discrepancy in Δv usage is now only 940 cm/s. Hence, as expected, it is always possible to improve the agreement between the two software sets by improving the modeling fidelity of all thrust arcs.

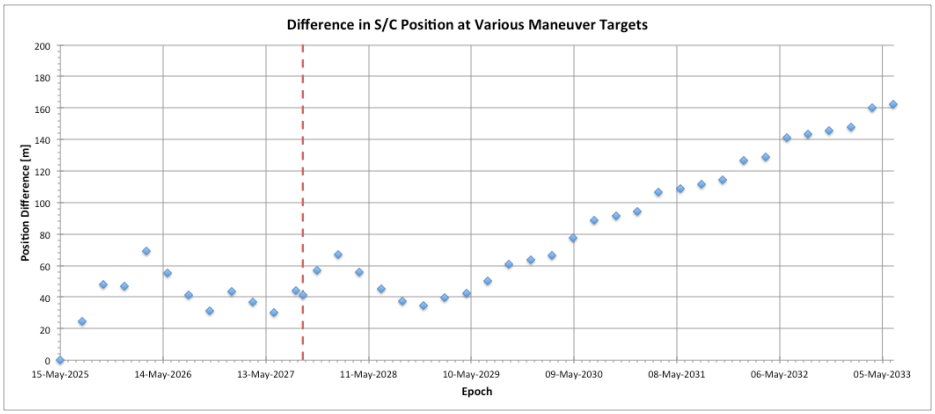

Figure 7: Differences in propagated spacecraft position of MIRAGE relative to EMTG for the Earth-Nauplius phase after thrust segment partition.

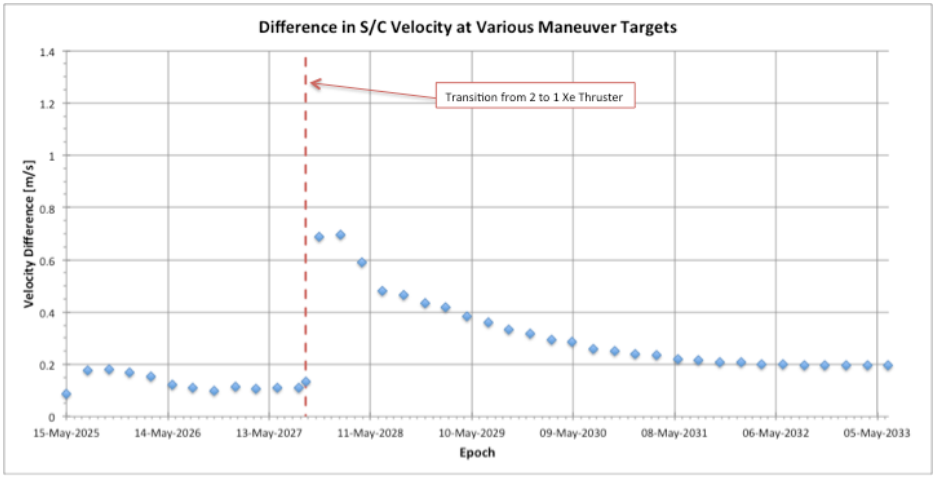

Figure 8: Differences in propagated spacecraft velocity of MIRAGE relative to EMTG for the Earth-Nauplius phase after thrust segment partition.

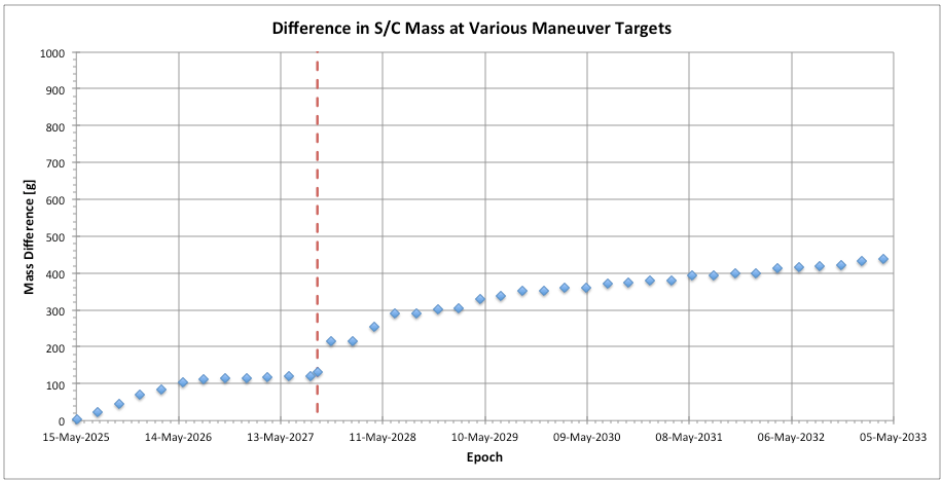

Figure 9: Differences in propagated spacecraft mass of MIRAGE relative to EMTG for the Earth-Nauplius phase after thrust segment partition.

Figures 10-12 show similar data for the Nauplius-Odysseus trajectory phase. There were no thruster mode changes within any thrust arcs over this phase, so consequently the agreement between EMTG and MIRAGE was somewhat improved, with a final mass discrepancy of 542 g, and a difference of only 14 mm/s out of 1.63 km/s of total Δv expended, again well within operational tolerances.

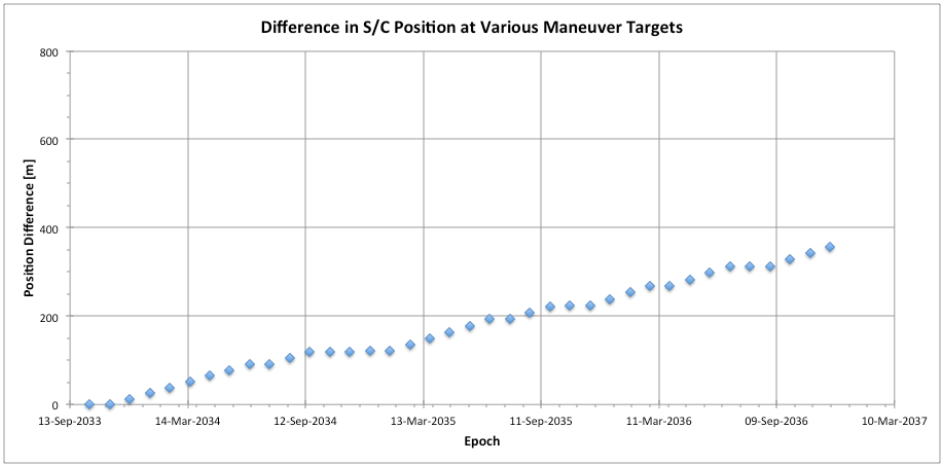

Figure 10: Differences in propagated spacecraft position of MIRAGE relative to EMTG for the Nauplius-Odysseus phase.

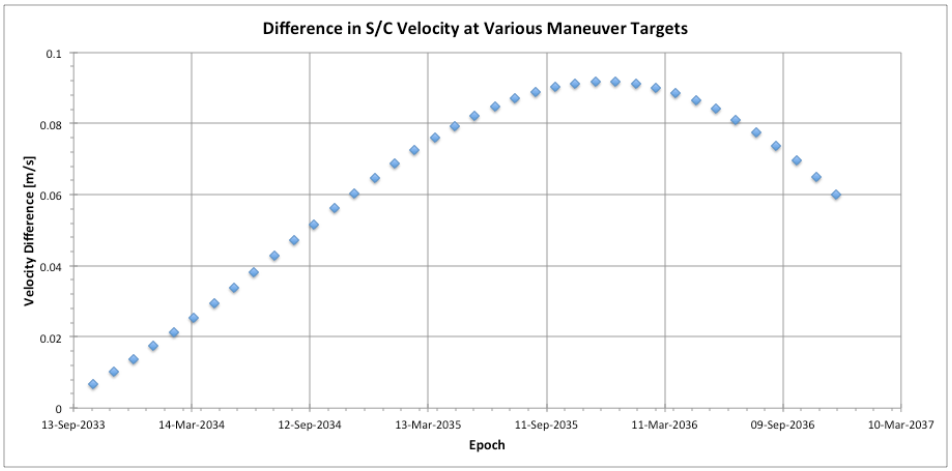

Figure 11: Differences in propagated spacecraft velocity of MIRAGE relative to EMTG for the Nauplius-Odysseus phase.

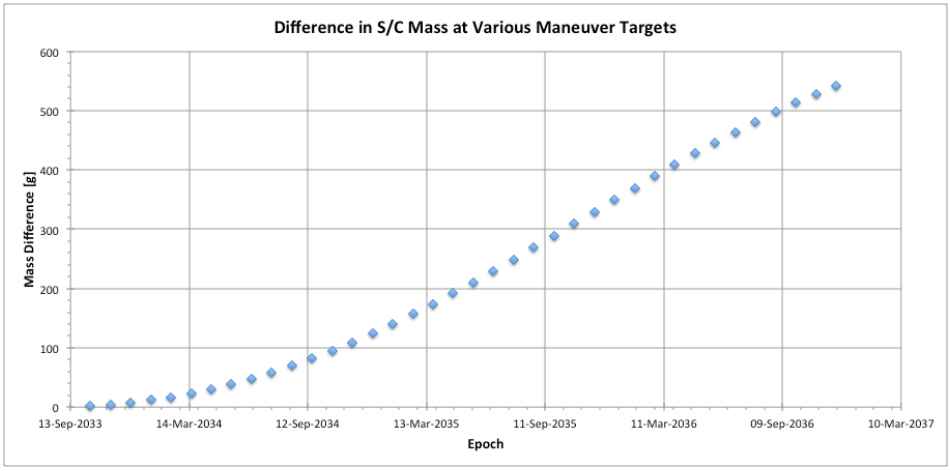

Figure 12: Differences in propagated spacecraft mass of MIRAGE relative to EMTG for the Nauplius-Odysseus phase.

APPROACH NAVIGATION: NAUPLIUS

The Nauplius approach navigation phase begins approximately 90 days from the encounter, with the goal of delivering the spacecraft to the pre-determined, asteroid-relative target. The dominant error source affecting the delivery accuracy is the *a priori* uncertainty in Nauplius's ephemeris, as determined from Earth-based observations. Incorporating images of Nauplius taken from the spacecraft into the OD solution is referred to as optical navigation (OpNav). OpNav can reduce the spacecraft-Nauplius relative position uncertainty, enabling a lower flyby altitude and improved science observations, thus making OpNav a priority on the approach. A flyby altitude of 1000 km was chosen for this analysis.

OpNav provides a measurement of the right ascension and declination of the center of Nauplius as seen from the spacecraft. Several factors affect our ability to determine Nauplius's center-of-mass, and hence its ephemeris, accurately. These include Nauplius being a small, dark body of unknown shape, with images being taken at a 45-49 degree solar phase angle from a moving platform with inherent pointing instability and pointing knowledge errors. Figure 13 shows a simulated OpNav image 30 days from the Nauplius encounter to illustrate the center-finding challenge. A discussion of center-finding is beyond the scope of this paper. For additional information on OpNav and the center-finding problem, we refer the interested reader to a recent paper by Jackman and Dumont [14].

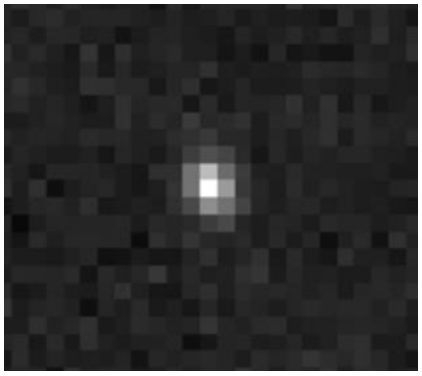

Figure 13: Simulated image of Nauplius 30 days from closest approach.

Using a heritage OpNav imager with an angular resolution of 5 μrad/pixel, Nauplius subtends more than 1 pixel only 34 days prior to the encounter, when the apparent magnitude is approximately 10. Figure 14 and 15 show the number of pixels subtended by Nauplius, and the apparent magnitude, as seen from the spacecraft, respectively. Figure 16 shows the spacecraft range to Nauplius during the approach.

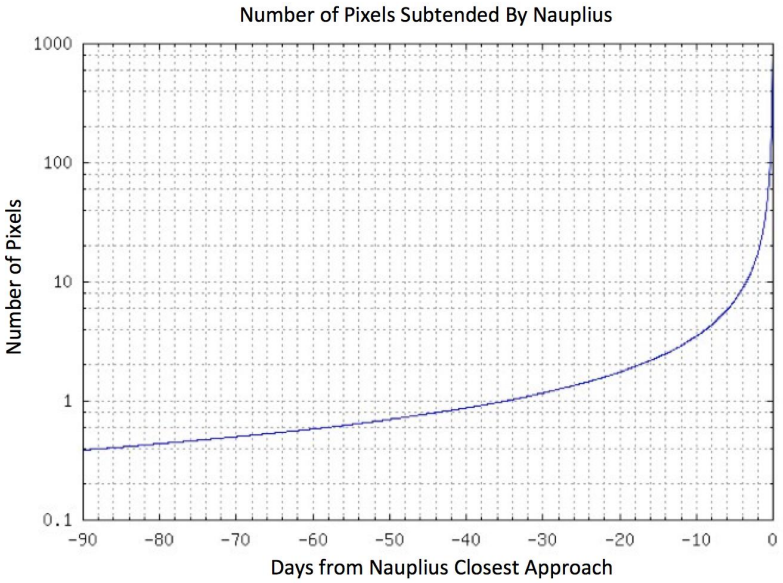

Figure 14: Number of pixels subtended by Nauplius during approach.

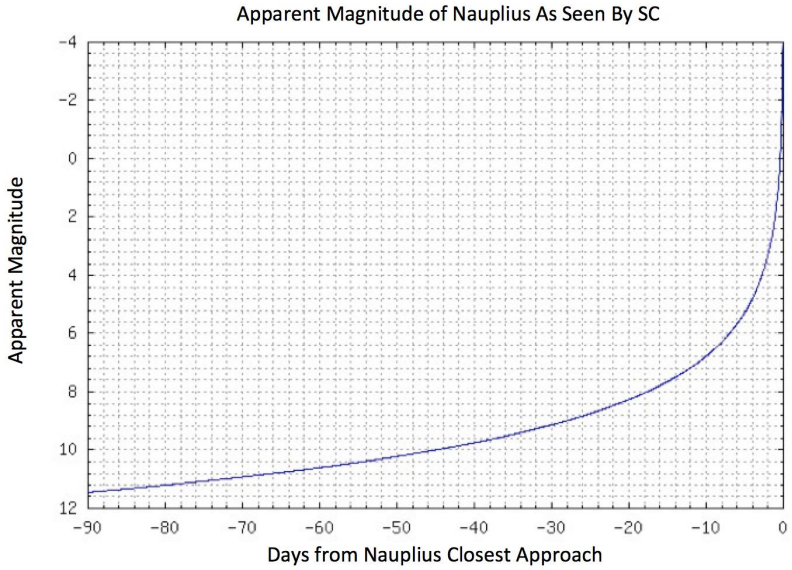

Figure 15: Apparent magnitude of Nauplius as seen by the spacecraft during approach.

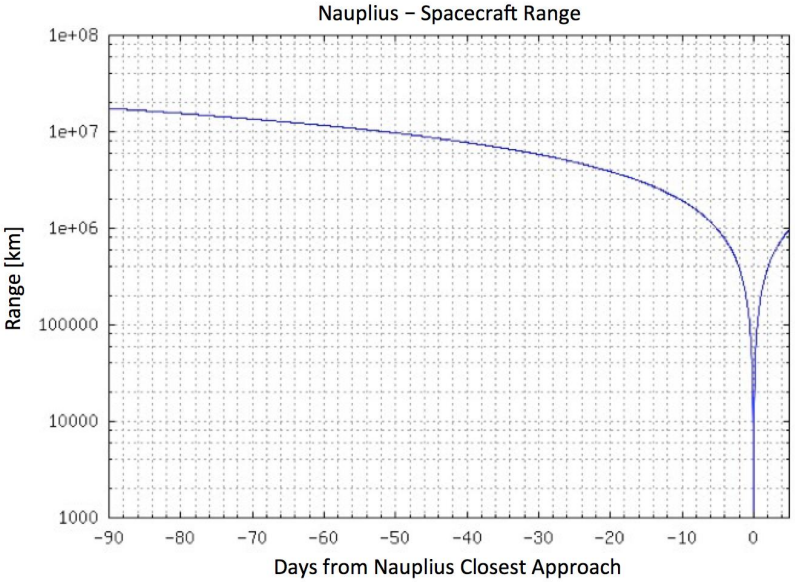

Figure 16: Spacecraft range from Nauplius during approach.

From Figure 16, at 30 days prior to the encounter (N-30), the spacecraft range is about 6 million km, so one pixel in the imager subtends an arc length of about 30 km at Nauplius. An apparent magnitude of 10 and a size of 1 pixel are used to provide a rough indication of when OpNavs begin improving the OD solution enough to consider a trajectory correction. We can see that this occurs for Nauplius between N-40 and N-30. For this reason, we plan an initial trajectory correction maneuver for this analysis at N-30 days. During the next three weeks, the center-finding progressively improves and maneuver opportunities will be scheduled periodically. The last planned targeting maneuver is at N-7 days, balancing the continual improvement in the OD solution with the operational constraints in planning and executing a maneuver late in the approach. OD solution refinements continue after the N-7 day maneuver, and a knowledge update (i.e. updating the spacecraft with the current spacecraft and Nauplius ephemerides), will be done on N-4 days. A final such update is incorporated into the schedule at N-3 days, but will only be used in case of an emergency. For example, if an unknown satellite of Nauplius is discovered, or some other anomalous event occurs.

In addition to OpNav images, radiometric tracking data from the Deep Space Network (DSN) is used to provide observations of the spacecraft motion with respect to the Earth. Two-way range and Doppler data provide a direct measurement of the line-of-sight range and range-rate, respectively. Position information normal to the line-of-sight, with respect to the Earth, is obtained using Delta Differential One-way Range (DDOR). This doubly-differenced very long baseline interferometry (VLBI) measurement uses two widely spaced DSN stations to alternately receive signals from the spacecraft and a quasar, which is chosen to be in close angular proximity to the spacecraft, producing a highly accurate measurement of the angular offset of the quasar to the baseline connecting the two DSN antennas. This combination of range, Doppler and DDOR provide measurements of the spacecraft position both in the line-of-sight and perpendicular to it, effectively resolving the position of the spacecraft relative to the Earth, while OpNav is used to determine the position of Nauplius relative to the spacecraft.

To better quantify the approach targeting knowledge uncertainties, a detailed covariance analysis was performed for the Nauplius encounter. Table 5 shows the covariance analysis assumptions. The following data schedule was assumed:

- Doppler/range
  - N-90 to N-60: three eight-hour passes per week

  - N-60 to encounter: one eight-hour pass per day

- DDOR
  - N-90 to encounter: Two east/west and two north/south baselines per week

- OpNav (eight images per "set")
  - N-60 to N-45: three image sets per week
  - N-45 to encounter: one image set per day

Table 5: Covariance analysis assumptions

Estimated parameters	***A priori* uncertainty**
spacecraft state	200 km, 30 m/s in each component
solar pressure	70 m^2 cross-sectional area (10 % of nominal value)
stochastic acceleration	1.0×10^{-12} km/s^2 constant bias (one day batch size)
maneuver execution error	30 mm/s (fixed) + 4% magnitude (assume 0.5 m/s in this analysis)
momentum dump maneuvers	0.5 mm/s per maneuver
Nauplius ephemeris	correlated covariance
Considered parameters	***A priori* uncertainty**
DSN station locations	0.5 m
UT1 and polar motion	15 cm and 10 cm
troposphere (wet/dry)	4 cm / 1 cm
ionosphere (wet/dry)	5 cm / 1 cm
μ	25%
Data type	**Data weight**
two-way Doppler	1 mm/s
two-way range	100 m
DDOR	0.2 ns
OpNav	four pixels prior to N-15 days, one pixel N-15 to encounter

Nauplius's gravitational parameter μ was calculated assuming a 33 km diameter spherical body with a density of $1 g/cm^3$. For the solar radiation pressure calculation, the spacecraft was assumed to have a sun-facing cross-sectional area of 114 m^2. Large solar arrays are necessary for sufficient electrical power. Correction maneuvers were assumed at N-30 and N-7 days, and momentum dumps were assumed every two weeks to desaturate the momentum wheels.

Using the covariance analysis, a maneuver schedule was determined. In general, if the current OD shows that the spacecraft is outside the 1σ error ellipse, a maneuver would be performed. The current maneuver schedule is provided in Table 6.

Table 6: Nauplius maneuver schedule

N - 60 days	- Placeholder to correct for large initial OD error.
	- Unlikely to be used since OpNav is minimally effective at this point.
N - 30 days	- First planned correction maneuver.
	- OpNav will have somewhat decreased the uncertainty in Nauplius's ephemeris by this time.
N - 7 days	- Final planned maneuver.
	- OpNav will have greatly reduced the targeting uncertainty by this time.
N - 3 days	- Final maneuver opportunity.
	- Unlikely to be used, except in an emergency, for example, should a Nauplius satellite be found.

The OD data cutoff for planning a correction maneuver is typically three days prior to maneuver execution. Since actionable improvement in the Nauplius ephemeris occurs late in the approach as discussed below, chemical propulsion is deemed necessary as SEP lacks the necessary thrust to make large corrections shortly before the encounter. The closest-approach flyby B-plane 3σ parameter uncertainty is shown in Figure 17.

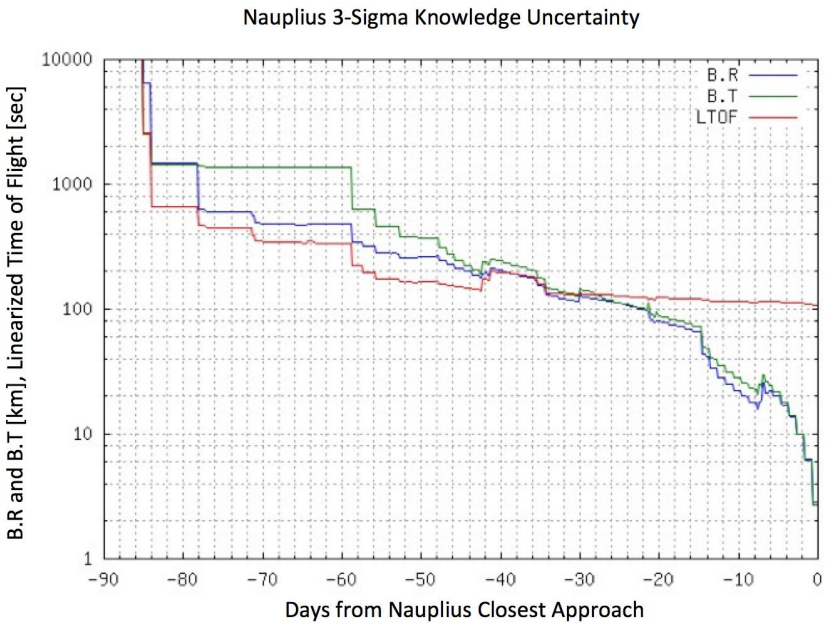

Figure 17: Spacecraft 3σ B-plane uncertainty during Nauplius approach.

Note that the linearized time-of-flight (LTOF) uncertainty (roughly the uncertainty in the time of arrival) remains stubbornly large throughout the approach. This is because one must be able to observe the parallax of Nauplius to improve the uncertainty in this direction, but the parallax is not observable until very late in the approach. This can be mitigated by including an auto-tracking camera for use, by performing a late update maneuver, or by providing the spacecraft with a new ephemeris for its state as well as one for Nauplius's state late in the approach for updating the camera pointing.

APPROACH NAVIGATION: ODYSSEUS

The approach to Odysseus is a simpler operation than the Nauplius flyby, in terms of reducing the spacecraft-asteroid relative state uncertainty. The relative velocity is less than 0.1 km/s and decreasing at Odysseus-60 (O-60), versus the spacecraft-Nauplius relative speed of 2.224 km/s. Odysseus is also nearly four times as large as Nauplius, subtending 100 pixels 60 days from rendezvous. The optical navigation problem becomes one of center-finding on an extended body, which was also discussed by Jackman and Dumont [14]. The uncertainties normal to the direction of motion can be resolved to a much higher accuracy than for the Nauplius flyby, while still a month or more from Odysseus closest approach. For this reason, a lower closest approach altitude of 400 km was chosen to enable more detailed science observations.

Figures 18-21 show the number of pixels subtended by Odysseus, its apparent magnitude as seen by the spacecraft, the spacecraft range from Odysseus and their relative speed during the last 90-days of the approach.

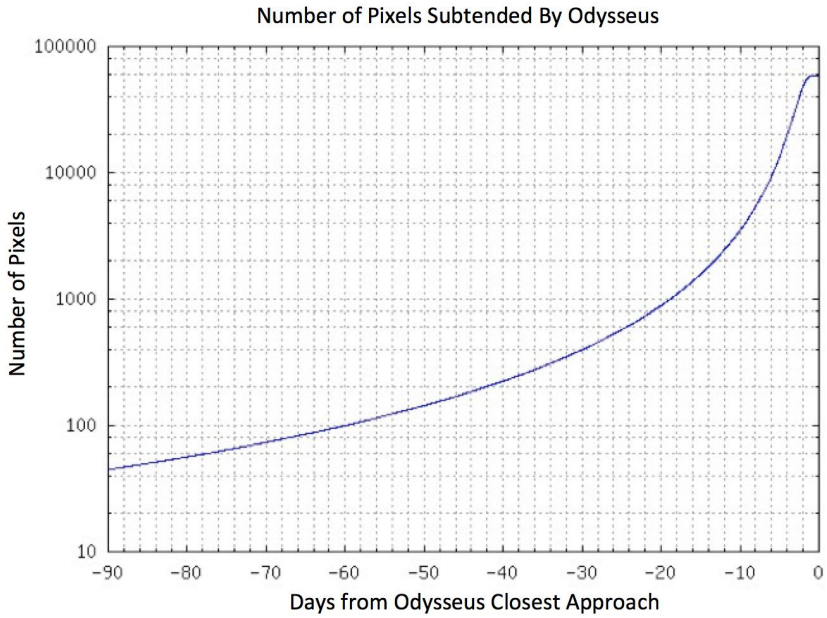

Figure 18: Number of pixels subtended by Odysseus during approach.

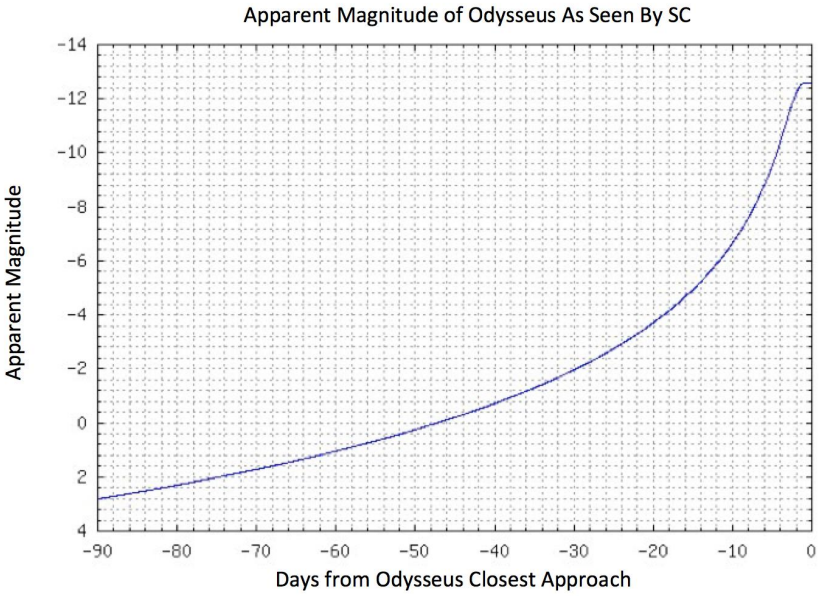

Figure 19: Apparent magnitude of Odysseus as seen by the spacecraft during approach.

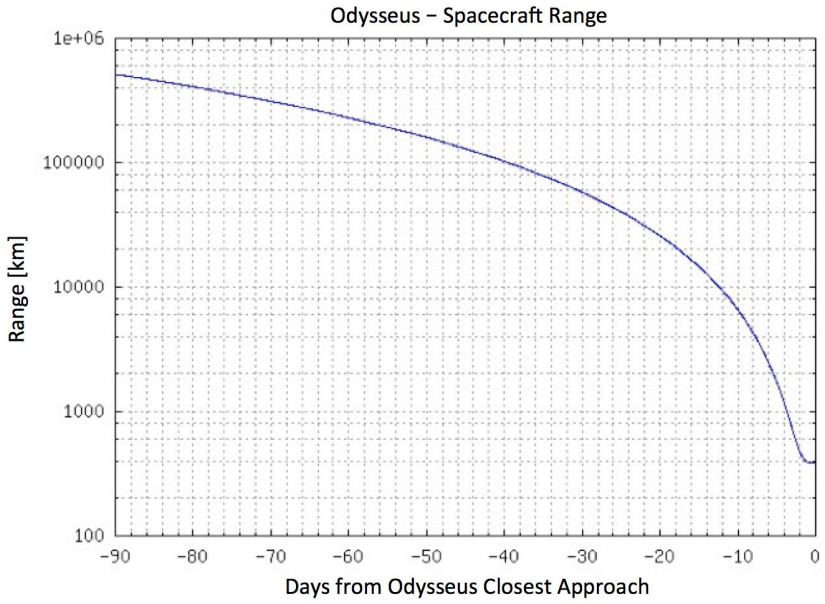

Figure 20: Spacecraft range from Odysseus during approach.

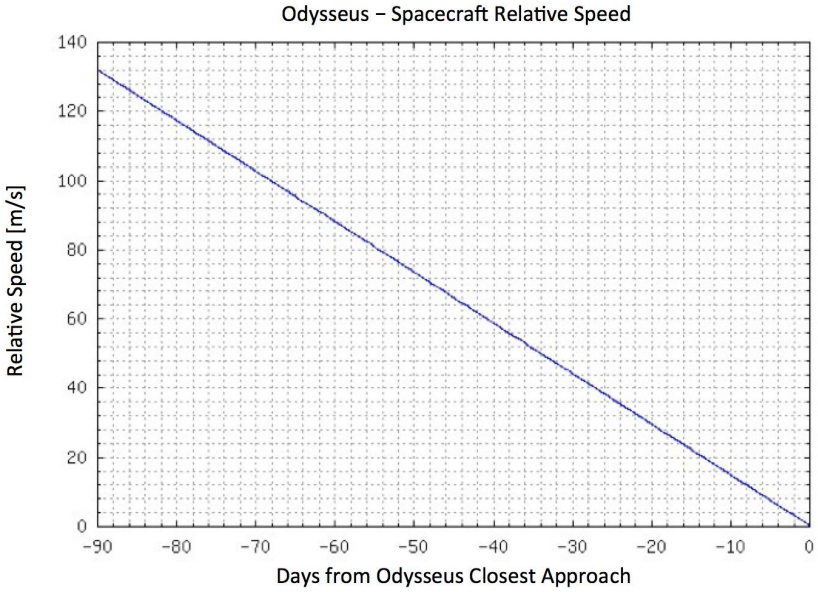

Figure 21: Spacecraft range from Odysseus during approach.

A covariance analysis was performed for the Odysseus approach using the same assumptions as given for the Nauplius flyby in Table 5, with the exception of the OpNav weighting due to the large number of pixels subtended by Odysseus. The OpNav weighting was chosen conservatively as 1 pixel from O-90 to O-30 days, and then 10 pixels from O-30 days until the encounter, when the extended body size exceeds 300 pixels. The covariance analysis B-plane knowledge uncertainties are shown in Figure 22.

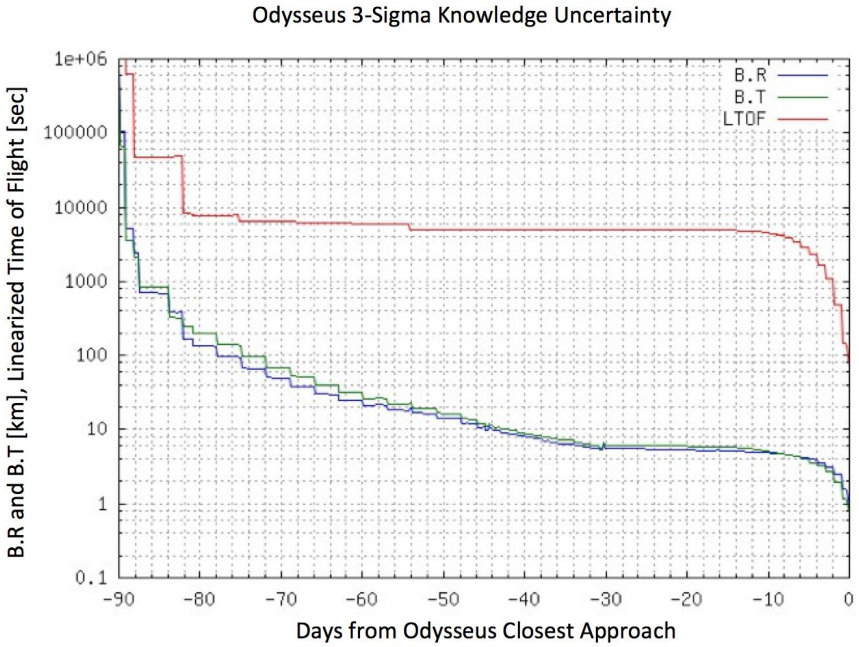

Figure 22: Spacecraft 3σ B-plane uncertainty during Odysseus approach.

Note that in this case, the time-of-flight uncertainty remains large on the approach, but it does go down rapidly in the last few days of the approach. With the low approach speed, there will be ample time to react and adjust the constant thrust vector to achieve the rendezvous target aim-point. Uncertainties in B.R and B.T are below 10 km as far out as 30 days prior to closest approach. Chemical propulsion, while useful, is not necessary for the Odysseus rendezvous.

CONCLUSION

This work describes validation of the medium-high fidelity interplanetary trajectory design tool EMTG against the high-fidelity flight navigation tool MIRAGE. The analysis presented here shows that an EMTG solution to a low-thrust interplanetary trajectory design problem may be trusted in a proposal or flight design. Furthermore, a validation process was developed and is now available for all future designs.

The second half of this work describes a notional mission to the Trojan asteroids 9712 Nauplius and 1143 Odysseus. This example is used to validate the low-thrust trajectory and also to develop a concept-of-operations for OpNav during the approach to the targets. The OpNav analysis shows that the low-velocity flyby of 9712 Nauplius is very achievable, as is the rendezvous with 1143 Odysseus. However, the OpNav analysis also shows that a SEP flyby mission would need to have the ability to perform a (relatively) high-thrust TCM after the last pre-flyby OpNav update and would therefore require a small chemical propulsion system. This can be done with the attitude control system thrusters. Most importantly, the example mission demonstrates that the EMTG-MIRAGE toolchain is adequate to propose and fly interplanetary SEP missions.

REFERENCES

[1] J. A. Englander, B. A. Conway, and T. Williams, "Automated Mission Planning via Evolutionary Algorithms," *Journal of Guidance, Control, and Dynamics*, Vol. 35, nov 2012, pp. 1878–1887, 10.2514/1.54101.

[2] J. A. Englander and B. A. Conway, "An Automated Solution of the Low-Thrust Interplanetary Trajectory Problem," *Journal of Guidance, Control, and Dynamics*, 2016. Accepted.

[3] J. Sims, P. Finlayson, E. Rinderle, M. Vavrina, and T. Kowalkowski, "Implementation of a Low-Thrust Trajectory Optimization Algorithm for Preliminary Design," *AIAA/AAS Astrodynamics Specialist Conference and Exhibit*, AIAA Paper 2006-6746, August 2006, 10.2514/6.2006-6746.

[4] T. T. McConaghy, *GALLOP Version 4.5 User's Guide*. School of Aeronautics and Astronautics, Purdue University, 2005.

[5] "PaGMO (Parallel Global Multiobjective Optimizer)," `https://github.com/esa/pagmo`, accessed 6/26/2016.

[6] C. Ocampo, *Elements of a Software System for Spacecraft Trajectory Optimization*, pp. 79–111. Cambridge University Press, 2010.

[7] G. J. Whiffen, "Mystic: Implementation of the Static Dynamic Optimal Control Algorithm for High-Fidelity, Low-Thrust Trajectory Design," *AIAA/AAS 2006-6741 Astrodynamics Specialist Conference and Exhibit*, Keystone, Colorado, August 21-24 2006.

[8] J. A. Englander, D. H. Ellison, and B. A. Conway, "Global Optimization of Low-Thrust, Multiple-Flyby Trajectories at Medium and Medium-High Fidelity," *AAS/AIAA Space-Flight Mechanics Meeting, Santa Fe, NM*, AAS, January 2014.

[9] P. J. Breckheimer, "DPTRAJ/ODP - DOUBLE PRECISION TRAJECTORY ANALYSIS AND ORBIT DETERMINATION PROGRAM," tech. rep., NASA, February 1994.

[10] D. Vallado, *Fundamentals of Astrodynamics and Applications Fourth Edition*. Microcosm Press, 2013.

[11] M. Vavrina and K. Howell, "Global Low-Thrust Trajectory Optimization Through Hybridization of a Genetic Algorithm and a Direct Method," *AIAA/AAS Astrodynamics Specialist Conference and Exhibit*, AIAA, aug 2008, 10.2514/6.2008-6614.

[12] "Announcement of Opportunity: New Frontiers 4, NNH16ZDA011O," `newfrontiers.larc.nasa.gov`, December 2016.

[13] "NASAs Evolutionary Xenon Thruster (NEXT): Ion Propulsion GFE Component Information Summary for Discovery Missions, July 2014," `http://discovery.larc.nasa.gov/discovery/pdf_files/20-NEXT-C_AO_Guidebook_11July14.pdf`, July 2014.

[14] C. D. Jackman and P. J. Dumont, "AAS 13-443 Optical Navigation Capabilities for Deep Space Missions," 23^{rd} *AAS/AIAA Space Flight Mechanics Meeting, Kauai HI*, February 10-14 2013.